Supporting Information for

Short Photoluminescence Lifetimes in Vacuum-Deposited $CH_3NH_3PbI_3$ Perovskite Thin Films as a Result of Fast Diffusion of Photogenerated Charge Carriers

Vladimir S. Chirvony[1,2]*, Kairolla S. Sekerbayev[3], Daniel Pérez-del-Rey[1], Juan P. Martínez-Pastor[2], Francisco Palazon[1], Pablo P. Boix[1], Toktar I. Taurbayev[3], Michele Sessolo[1], and Henk J. Bolink[1]

[1]Instituto de Ciencia Molecular, Universidad de Valencia, c/Catedrático J. Beltrán, 2, Paterna 46980, Spain; [2]UMDO (Unidad de Materiales y Dispositivos Optoelectrónicos), Instituto de Ciencia de los Materiales, Universidad de Valencia, Valencia 46071, Spain; [3]Institute of Experimental and Theoretical Physics, Al-Farabi Kazakh National University, Almaty, 050040 Kazakhstan

Corresponding Author

vladimir.chyrvony@uv.es

Table of Content

Materials and Methods……..……..…….……3-5

Note 1: Evaluation of maximum permissible concentrations of carriers to avoid bimolecular recombination……...……...…...6-7

Figure S1……..….7

Figure S2…… ……..8

Figure S3……...9

Note 2: Analysis of PL transients modeled by one-dimensional linear diffusion equation ……..……...…….....9-10

References……....10

Materials and methods

Fabrication of solar cell and $CH_3NH_3PbI_3$ layers. Photolithographically patterned ITO coated glass substrates were purchased from Naranjo Substrates. N4,N4,N4″,N4″-tetra([1,1′-biphenyl]-4-yl)-[1,1′:4′,1″-terphenyl]-4,4″-diamine (TaTm) were provided from Novaled GmbH. TiO_2 nanoparticle suspensions were prepared in IMEC following the preparation procedure explained in reference 2. Fullerene (C60) and TOPO were purchased from sigma Aldrich. PbI_2 was purchased from Tokyo Chemical Industry CO (TCI), CH_3NH_3I (MAI), MoO_3 and BCP were purchased from Lumtec. ITO prepatterned substrates (for solar cells) and merely glass substrates were cleaned following a standard procedure where they are cleaned with soap, water, deionized water and isopropanol in a sonication bath, followed by a 20 min UV treatment. The TiO_2 dispersion was deposited in air by spin-coating at 3000 rpm for 30 s and annealed at 100 °C for 30 min, leading to a 50−80 nm thick compact layer. Then, the samples were transferred to a vacuum chamber integrated into a nitrogen-filled glovebox (H_2O and O_2 < 0.1 ppm) and evacuated to a pressure of 10^{-6} mbar. The vacuum chamber is equipped with six temperature-controlled evaporation sources (Creaphys) fitted with ceramic crucibles. The sources were directed upward with an angle of approximately 90° with respect to the bottom of the evaporator. The substrate holder to evaporation sources distance is approximately 20 cm. Three quartz crystal microbalance (QCM) sensors are used: two monitoring the deposition rate of each evaporation source and a third one close to the substrate holder monitoring the total deposition rate. For thickness calibration, we individually sublimed the charge transport materials. A calibration factor was obtained by comparing the thickness inferred from the QCM sensors with that measured with a mechanical profilometer (Ambios XP1). Then, the materials were sublimed at temperatures ranging from 160 ºC to >300 ºC, and the evaporation rate was controlled by separate QCM sensors obtaining precisely the

deposited thickness. In general, the deposition rate for TaTm, C60 and BCP was 0.5 Å s^{-1}. For the perovskite deposition, MAI and PbI_2 were coevaporated by measuring the deposition rate of each material in a different sensor and obtaining the total perovskite thickness in a third one, leading to 500 nm thick perovskite. MoO_3, Ag and Au were evaporated in a second vacuum chamber with the same working principle as the first one previously described, using aluminum boats as sources. TOPO was deposited in a nitrogen filled glovebox by spin coating a 20 mM solution using toluene as solvent. For the solar cell characterization, the external quantum efficiency (EQE) was estimated using the cell response at different wavelengths (measured with a white light halogen lamp in combination with band-pass filters), where the solar spectrum mismatch is corrected using a calibrated Silicon reference cell (MiniSun simulator by ECN, The Netherlands). The J−V characteristics were obtained using a Keithley 2400 source measure unit and under white light illumination, and the short-circuit current density was corrected considering the device EQE. The electrical characterization was validated using a solar simulator by Abet Technologies (model 10500 with an AM1.5G xenon lamp as the light source). Before each measurement, the exact light intensity was determined using a calibrated Si reference diode equipped with an infrared cutoff filter (KG-3, Schott). The J−V curves were recorded between −0.2 and 1.2 V with 0.01 V steps, integrating the signal for 20 ms after a 10 ms delay. This corresponds to a speed of about 0.3 V s^{-1}. The layout used to test the solar cells has four equal areas (0.0653 cm^2, defined as the overlap between the ITO and the top metal contact) and measured through a shadow mask with 0.01 cm^2 aperture.

PL measurements. Time-resolved PL (TRPL) kinetics were measured by pumping the sample with a 200 fs pulsed Ti:sapphire (Coherent Mira 900D) at a repetition rate of 76

MHz doubled to 405 nm with a BBO crystal. The backscattered PL signal was dispersed by a double 0.3-m focal length grating spectrograph/spectrometer (1200 g/mm with 750 nm blaze) and detected by a Si micro photon device (MPD) single-photon avalanche diode (SPAD) photodetector (connected through a multimode optical fiber to the monochromator); the SPAD was attached to a time correlated single photon counting electronic board (TCC900 from Edinburgh Instruments). The instrument response function is about 50 ps.

Note 1: Evaluation of maximum permissible concentrations of carriers to avoid bimolecular recombination

It is easy to show by simple calculations what are the maximum permissible magnitudes of the carrier concentration *n* to avoid an influence of bimolecular recombination in cases of ~1 ns and ~100 ns PL lifetimes. Indeed, the rate of the carrier concentration decay after photoexcitation $\frac{dn}{dt}$ can be written as a sum of three processes [1, 2]:

$$\frac{dn}{dt} = -(k_1 n + k_2 n^2 + k_3 n^3), \quad (1)$$

where k_1, k_2, and k_3 are the constants of a monomolecular, bimolecular, and Auger recombination, respectively. On the basis of eq. (1), the expression (2) can be written:

$$\left.\frac{dn}{dt}\right/_n = -(k_1 + k_2 n + k_3 n^2), \quad (2)$$

which describes the instantaneous rate of the PL decay (in s^{-1}) at a given carrier concentration *n*. Note that an analogous term $r(n) = k_1 + k_2 n + k_3 n^2$ named as "the total recombination rate" has been recently considered in literature [3]. The first term prevails at low *n*, whereas a role of other two terms increases with *n* and, in general, is determined by the k_2 and k_3 coefficients. The value of k_2 for bulk carrier recombination in MAPI is of the order of 10^{-9} см^3 с$^{-1}$ as a maximum [4]. For example, in case of excitation with n=10^{16} – 10^{17} cm^{-3} it results in $k_2 n$ = 10^7 – 10^8 s^{-1}. It implies that the PL transient with τ_{PL} ~ 1 ns, which is observed for non-passivated eMAPI layers, cannot be influenced by the bimolecular recombination process at these carrier concentrations. However, if the experimentally measured PL kinetics is of the order of 100 ns (the case of passivated eMAPI layer), analogous evaluations show that the concentration interval to avoid

bimolecular processes is now $10^{14} – 10^{15}$ cm^{-3}. This is why we measured the PL kinetics for non-passivated and passivated eMAPI layers at different excitation densities corresponding to n ~ 10^{16} cm^{-3} and ~ 10^{15} cm^{-3}, respectively. When we increased *n* higher than n ~ 10^{15} cm^{-3} for the case of passivated layer, the PL kinetics shortened (see Fig. S1). Note that the term k_3n^2 is not considered here at all because at n=$10^{15} – 10^{16}$ cm^{-3} and k_3 = 10^{-28} $s^{-1}cm^{-6}$ [5, 6] the term $k_3n^2 = 10^2 – 10^4$ s^{-1} that makes influence of the Auger

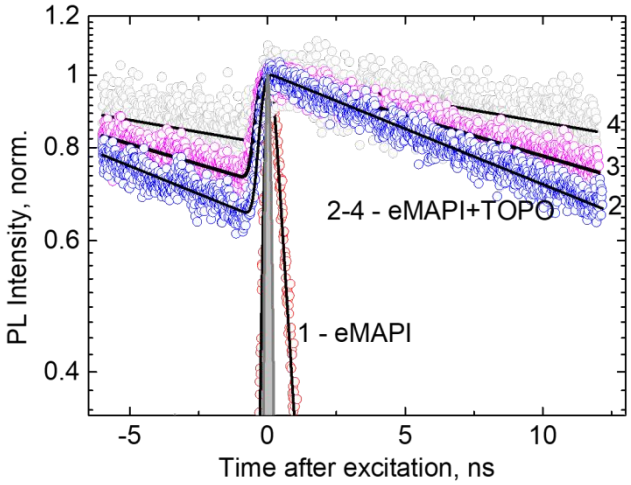

recombination on the 1 – 100 ns PL kinetics completely negligible.

Figure S1. Experimental PL kinetics (symbols) and fitting (lines) measured for pristine (curve 1, τ_{PL} = 0.75 ns) and TOPO-passivated eMAPI layers at photogenerated carrier concentrations of $1.44 \cdot 10^{16}$ (curve 2, τ_{PL} = 30.2 ns), $6.3 \cdot 10^{15}$ (curve 3, τ_{PL} = 41.5 ns), and

$1.0 \cdot 10^{15}$ cm^{-3} (curve 4, τ_{PL} = 73.5 ns). The instrument response function is shown as a filled gray contour.

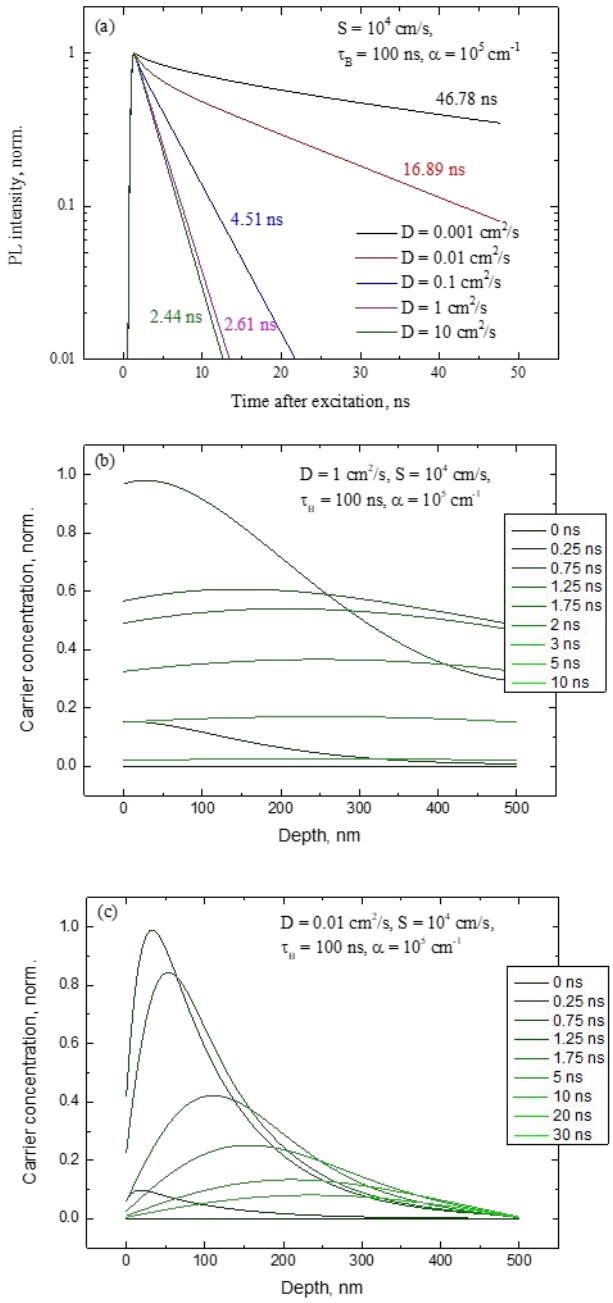

Figure S2. Model PL transients (a) and carrier concentration distributions at different times after excitation by 100 fs pulses (b and c) calculated for non-passivated MAPI layers possessing the parameters indicated in the figure legends.

Note 2: Analysis of PL transients modeled by one-dimensional linear diffusion equation

When modelling PL transients by the diffusion equation (equation (1) in the manuscript) for the case of repetitive excitation with the time interval T between pulses and $T < \tau_{PL}$ we consistently calculated each excitation cycle. The initial value of the concentration of the next calculation cycle was taken as the final value of the previous one. Cycles are calculated until an equilibrium is established, i.e. when the carrier concentration profile does not change when calculating a new cycle. Fig. S2 demonstrates the results of our modeling of such a transient process for the case of the TOPO-passivated 500-nm layers with D = 1 cm^2/s and S = 120 cm/s.

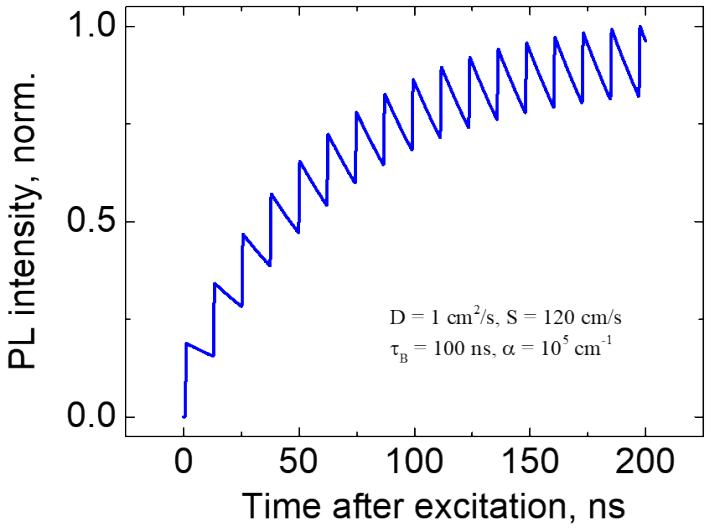

Figure S3. Model PL transient calculated by diffusion equation for TOPO-passivated eMAPI layer with $D = 1 cm^2/s$, $S_{eff} = 120$ cm/s, $\tau_B = 100$ ns, and $\alpha = 10^5$ cm^{-1} for the first 200 ns after starting excitation by train of 100-fs pulses.

References

1. Stranks, S. D.; Burlakov, V. M.; Leijtens, T.; Ball, J. M.; Goriely, A.; Snaith, H. J. Recombination kinetics in organic-inorganic perovskites: excitons, free charge, and subgap states. *Phys. Rev. Appl.* **2014**, *2*, 034007.

2. Yamada, Y.; Nakamura, T.; Endo, M.; Wakamiya, A.; Kanemitsu, Y. Photocarrier recombination dynamics in perovskite $CH_3NH_3PbI_3$ for solar cell applications. *J. Am. Chem. Soc.* **2014**, *136*, 11610-11613.

3. Herz, L. M. Charge-Carrier Dynamics in Organic-Inorganic Metal Halide Perovskites, *Annu. Rev. Phys. Chem.* **2016**, *67*, 65-89.

4. Crothers, T. W.; Milot, R. L.; Patel, J. B.; Parrott, E. S.; Schlipf, J.; Müller-Buschbaum, P.; Johnston, M. B.; Herz, L. M. Photon Reabsorption Masks Intrinsic Bimolecular Charge-Carrier Recombination in CH3NH3PbI3 Perovskite. *Nano Lett.* **2017**, *17*, 5782-5789.

5. Wehrenfennig, C.; Eperon, G. E.; Johnston, M. B.; Snaith, H. J.; Herz, L. M. High Charge Carrier Mobilities and Lifetimes in Organolead Trihalide Perovskites. *Adv. Mater.* **2014**, *26*, 1584-1589.

6. Yang, Y.; Yang, M.; Li, Z.; Crisp, R.; Zhu, K.; Beard, M. C. Comparison of Recombination Dynamics in $CH_3NH_3PbBr_3$ and $CH_3NH_3PbI_3$ Perovskite Films: Influence of Exciton Binding Energy. *J. Phys. Chem. Lett.* 2015, *6*, 4688-4692.